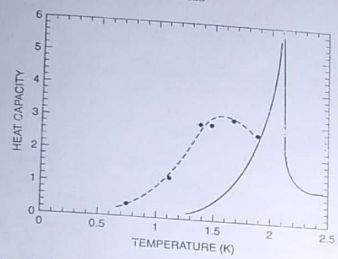

Figure 4.23. Specific heat versus temperature for liquid helium (solid line) and a liquid consisting of clusters of 64 helium atoms (dark circles). The peak corresponds to the transition to the superfluid state. [Adapted from P. Sindzingre, *Phys. Rev. Lett.* 63, 1601 (1989).]

When boson condensation occurs in liquid He^4 at the temperature 2.2 K, called the *lambda point* (λ point), the liquid helium becomes a superfluid, and its viscosity drops to zero. Normally when a liquid is forced though a small thin tube, it moves slowly because of friction with the walls, and increasing the pressure at one end increases the velocity. In the superfluid state the liquid moves quickly through the tube, and increasing the pressure at one end does not change the velocity. The transition to the superfluid state at 2.2 K is marked by a discontinuity in the specific heat known as the *lambda transition*. The specific heat is the amount of heat energy necessary to raise the temperature of one gram of the material by 1 K. Figure 4.23 shows a plot of the specific heat versus temperature for bulk liquid helium, and for a helium cluster of 64 atoms, showing that clusters become superfluid at a lower temperature than the bulk liquid of He atoms.

4.4.3. Molecular Clusters

Individual molecules can form clusters. One of the most common examples of this is the water molecule. It has been known since the early 1970s, long before the invention of the word *nanoparticle*, that water does not consist of isolated H_2O molecules. The broad Raman spectra of the O–H stretch of the water molecule in the liquid phase at 3200–3600 cm^{-1} has been shown to be duc to a number of overlapping peaks arising from both isolated water molecules and water molecules hydrogen-bonded into clusters. The H atom of one molecule forms a bond with the oxygen atom of another. Figure 4.24 shows the structure of one such water cluster. At ambient conditions 80% of water molecules are bonded into clusters, and as the

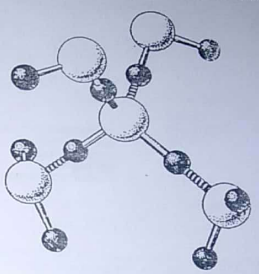

Figure 4.24. A hydrogen-bonded cluster of five water molecules. The large spheres are oxygen, and the small spheres are hydrogen atoms.

temperature is raised, the clusters dissociate into isolated H_2O molecules. In the complex shown in Fig. 4.24 the H atom is not equidistant between the two oxygens. Interestingly, it has been predicted that under 9 GPa of shock loading pressure a new form of water might exist called *symmetrically hydrogen-bonded water*, where the H atom is equally shared between both oxygens. It is possible that such water could have properties different from those of normal water. There are other examples of molecular clusters such as $(NH_3)_n^+$, $(CO_2)_{44}$ and $(C_4H_8)_{30}$.

4.5. METHODS OF SYNTHESIS

Earlier in the chapter we described one method of making nanoparticles using laser-evaporation in which a high intensity laser beam is incident on a metal rod, causing atoms to be evaporated from the surface of the metal. These metal atoms are then cooled into nanoparticles. There are, however, other ways to make nanoparticles, and we will describe several of them.

4.5.1. RF Plasma

Figure 4.25 illustrates a method of nanoparticle synthesis that utilizes a plasma generated by RF heating coils. The starting metal is contained in a pestle in an evacuated chamber. The metal is heated above its evaporation point using high voltage RF coils wrapped around the evacuated system in the vicinity of the pestle. Helium gas is then allowed to enter the system, forming a high temperature plasma

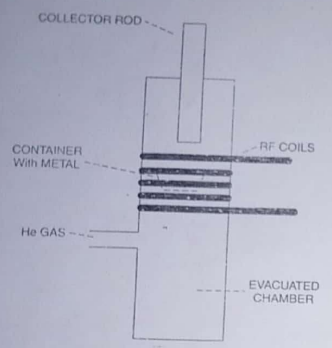

Figure 4.25. Illustration of apparatus for the synthesis of nanoparticles using an RF-produced plasma.

in the region of the coils. The metal vapor nucleates on the He gas atoms and diffuses up to a colder collector rod where nanoparticles are formed. The particles are generally passivated by the introduction of some gas such as oxygen. In the case of aluminum nanoparticles the oxygen forms a layer of aluminum oxide about the particle.

4.5.2. Chemical Methods

Probably the most useful methods of synthesis in terms of their potential to be scaled up are chemical methods. There are a number of different chemical methods that can be used to make nanoparticles of metals, and we will give some examples. Several types of reducing agents can be used to produce nanoparticles such as $NaBEt_3H$, $LiBEt_3H$, and $NaBH_4$, where Et denotes the ethyl ($-C_2H_5$) radical. For example, nanoparticles of molybdenum (Mo) can be reduced in toluene solution with $NaBEt_3H$ at room temperature, providing a high yield of Mo nanoparticles having dimensions of 1–5 nm. The equation for the reaction is

$$MoCl_3 + 3NaBEt_3H \Rightarrow Mo + 3NaCl + 3BEt_3 + (3/2)H_2 \qquad (4.9)$$

Nanoparticles of aluminum have been made by decomposing $Me_2EtNAlH_3$ in toluene and heating the solution to 105°C for 2 h (Me is methyl, $-CH_3$). Titanium

isopropoxide is added to the solution. The titanium acts as a catalyst for the reaction. The choice of catalyst determines the size of the particles produced. For instance, 80-nm particles have been made using titanium. A surfactant such as oleic acid can be added to the solution to coat the particles and prevent aggregation.

4.5.3. Thermolysis

Nanoparticles can be made by decomposing solids at high temperature having metal cations, and molecular anions or metal organic compounds. The process is called *thermolysis*. For example, small lithium particles can be made by decomposing lithium azide, LiN_3. The material is placed in an evacuated quartz tube and heated to 400°C in the apparatus shown in Fig. 4.26. At about 370°C the LiN_3 decomposes, releasing N_2 gas, which is observed by an increase in the pressure on the vacuum gauge. In a few minutes the pressure drops back to its original low value, indicating that all the N_2 has been removed. The remaining lithium atoms coalesce to form small colloidal metal particles. Particles less than 5 nm can be made by this method. Passivation can be achieved by introducing an appropriate gas.

The presence of these nanoparticles can be detected by electron paramagnetic resonance (EPR) of the conduction electrons of the metal particles. Electron paramagnetic resonance, which is described in more detail in Chapter 3, measures the energy absorbed when electromagnetic radiation such as microwaves induces a transition between the spin states m_s split by a DC magnetic field. Generally the experiment measures the derivative of the absorption as a function of an increasing DC magnetic field. Normally because of the low penetration depth of the microwaves into a metal, it is not possible to observe the EPR of the conduction electrons.

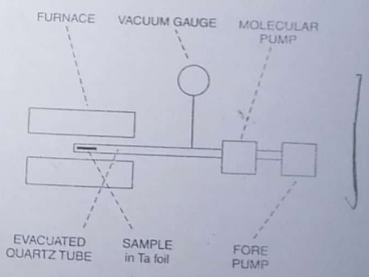

Figure 4.26. Apparatus used to make metal nanoparticles by thermally decomposing solids consisting of metal cations and molecular anions, or metal organic solids. (F. J. Owens, unpublished.)

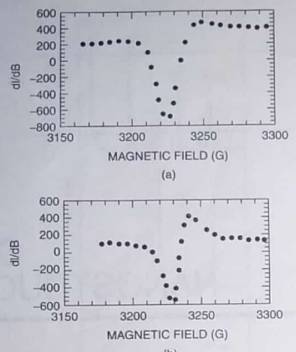

Figure 4.27. Electron paramagnetic resonance spectra at 300 K (a) and 77 K (b) arising from conduction electrons in lithium nanoparticles formed from the thermal decomposition of LiN_3. (F. J. Owens, unpublished.)

However, in a collection of nanoparticles there is a large increase in surface area, and the size is of the order of the penetration depth, so it is possible to detect the EPR of the conduction electrons. Generally EPR derivative signals are quite symmetric, but for the case of conduction electrons, relaxation effects make the lines very asymmetric, and the extent of the asymmetry is related to the small dimensions of the particles. This asymmetry is quite temperature dependent as indicated in Fig. 4.27, which shows the EPR spectra of lithium particles at 300 and 77 K that had been made by the process described above. It is possible to estimate the size of the particles from the *g*-factor shift and line width of the spectra.

4.5.4. Pulsed Laser Methods

Pulsed lasers have been used in the synthesis of nanoparticles of silver. Silver nitrate solution and a reducing agent are flowed through a blenderlike device. In the blender there is a solid disk, which rotates in the solution. The solid disk is subjected to pulses from a laser beam creating hot spots on the surface of the disk. The apparatus is illustrated in Fig. 4.28. Silver nitrate and the reducing agent react at these hot spots, resulting in the formation of small silver particles, which can be separated from the solution using a centrifuge. The size of the particles is controlled by the

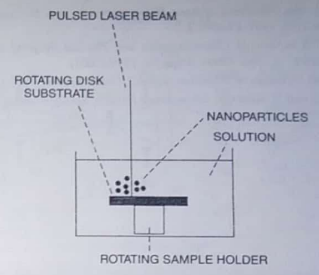

Figure 4.28. Apparatus to make silver nanoparticles using a pulsed laser beam that creates hot spots on the surface of a rotating disk. [Adapted from J. Singh, *Mater. Today* **2**, 10 (2001).]

energy of the laser and the rotation speed of the disk. This method is capable of a high rate of production of 2–3 g/min.

4.6. CONCLUSION

In this chapter a number of examples have been presented showing that the physical, chemical, and electronic properties of nanoparticles depend strongly on the number and kind of atoms that make up the particle. We have seen that color, reactivity, stability, and magnetic behavior all depend on particle size. In some instances entirely new behavior not seen in the bulk has been observed such as magnetism in clusters that are constituted from nonmagnetic atoms. Besides providing new research challenges for scientists to understand the new behavior, the results have enormous potential for applications, allowing the design of properties by control of particle size. It is clear that nanoscale materials can form the basis of a new class of atomically engineered materials.

FURTHER READING

R. P. Anders et al., "Research Opportunities in Clusters and Cluster Assembled Materials," *J. Mater. Res.* **4**, 704 (1989).

W. A. De Heer, "Physics of Simple Metal Clusters," *Rev. Mod. Phys.* **65**, 611 (1993).

M. A. Duncan and D. H. Rouvray, "Microclusters," *Sci. Am.* 110 (Dec. 1989).

S. N. Khanna, *Handbook of Nano Phase Materials*, in A N. Goldstein, ed., Marcel Decker, New York, 1997, Chapter 1.

J. Lue, "A Review of Characterization and Physical Property Studies of Metallic Nanoparticles," *J. Phys. Chem. Solids* **62**, 1599 (2001).

M. Morse, "Clusters of Transition Atoms," *Chem. Rev.* **86**, 1049 (1986).

S. Sugano and H. Koizumi, *Microcluster Physics*, Springer-Verlag, Heidelberg, 1998.

5

CARBON NANOSTRUCTURES

5.1. INTRODUCTION

This chapter is concerned with various nanostructures of carbon. A separate chapter is devoted to carbon because of the important role of carbon bonding in the organic molecules of life (see Chapter 12), and the unique nature of the carbon bond itself. It is the diverse nature of this bond that allows carbon to form some of the more interesting nanostructures, particularly carbon nanotubes. Possibly more than any of the other nanostructures, these carbon nanotubes have enormous applications potential which we will discuss in this chapter.

5.2. CARBON MOLECULES

5.2.1. Nature of the Carbon Bond

In order to understand the nature of the carbon bond it is necessary to examine the electronic structure of the carbon atom. Carbon contains six electrons, which are distributed over the lowest energy levels of the carbon atom. The structure is designated as follows $(1s)^2$, $(2s)$, $(2p_x)$, $(2p_y)$, $(2p_z)$ when bonded to atoms in molecules. The lowest energy level $1s$ with the quantum number $N = 1$ contains two

Introduction to Nanotechnology by Charles P. Poole Jr. and Frank J. Owens.
ISBN 0-471-07935-9.

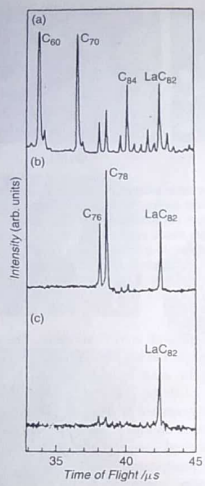

Figure 3.9. Time-of-flight mass spectra from soot produced by laser vaporization of a lanthanum–carbon target, showing the presence of the fullerene molecules C_{60}, C_{70}, C_{76}, C_{78}, C_{82}, C_{84}, and LaC_{84}. The spectra correspond, successively, to (a) the initial crude soot extract, (b) a fraction after passage through a chromatographic column, and (c) a second fraction after passage of the first fraction through another column to isolate and concentrate the endohedral compound LaC_{82}. [From K. Kikuchi, S. Suzuki, Y. Nakao, N. Yakahara, T. Wakabayashi, I. Ikemoto, and Y Achiba, *Chem. Phys. Lett.* **216**, 67 (1993).]

3.3. MICROSCOPY

3.3.1. Transmission Electron Microscopy

Electron beams not only are capable of providing crystallographic information about nanoparticle surfaces but also can be used to produce images of the surface, and they play this role in electron microscopes. We will discuss several ways to use electron beams for the purpose of imaging, using several types of electron microscopes.

In a transmission electron microscope (TEM) the electrons from a source such as an electron gun enter the sample, are scattered as they pass through it, are focused by

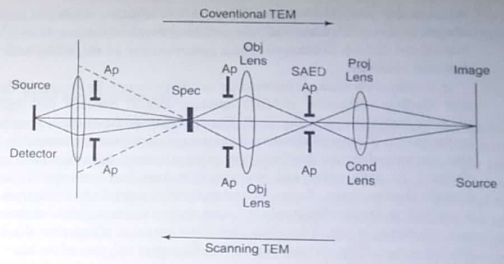

Figure 3.10. Ray diagram of a conventional transmission electron microscope (top path) and of a scanning transmission electron microscope (bottom path). The selected area electron diffraction (SAED) aperture (Ap) and the sample or specimen (Spec) are indicated, as well as the objective (Obj) and projector (Proj) or condenser (Cond) lenses. (Adapted from P. R. Buseck, J. M. Cowley, and L. Eyring, *High-Resolution Transmission Electron Microscopy*, Oxford Univ. Press, New York, 1988, p. 6.)

an objective lens, are amplified by a magnifying (projector) lens, and finally produce the desired image, in the manner reading from left to right (CTEM direction) in Fig. 3.10. The wavelength of the electrons in the incident beam is given by a modified form of Eq. (3.6)

$$\lambda = \frac{0.0388}{\sqrt{V}} \text{ nm} \tag{3.7}$$

where the energy acquired by the electrons is $E = eV$ and V is the accelerating voltage expressed in kilovolts. If widely separated heavy atoms are present, they can dominate the scattering, with average scattering angles θ given by the expression $\theta \sim \lambda/d$, where d is the average atomic diameter. For an accelerating voltage of 100 kV and an average atomic diameter of 0.15 nm, we obtain $\theta \sim 0.026$ radians or 1.5°. Images are formed because different atoms interact with and absorb electrons to a different extent. When individual atoms of heavy elements are farther apart than several lattice parameters, they can sometimes be resolved by the TEM technique.

Electrons interact much more strongly with matter than do X rays or neutrons with comparable energies or wavelengths. For ordinary elastic scattering of 100-keV electrons the average distance traversed by electrons between scattering events, called the *mean free path*, varies from a few dozen nanometers for light elements to tens or perhaps hundreds of nanometers for heavy elements. The best results are obtained in electron microscopy by using film thicknesses that are comparable with

the mean free path. Much thinner films exhibit too little scattering to provide useful images, and in thick films multiple scattering events dominate, making the image blurred and difficult to interpret. Thick specimens can be studied by detecting back-scattered electrons.

A transmission electron microscope can form images by the use of the selected-area electron diffraction (SAED) aperture located between the objective and projector lenses shown in Fig. 3.10. The main part of the electron beam transmitted by the sample consists of electrons that have not undergone any scattering. The beam also contains electrons that have lost energy through inelastic scattering with no deviation of their paths, and electrons that have been reflected by various *hkl* crystallographic planes. To produce what is called a *bright-field image*, the aperture is inserted so that it allows only the main undeviated transmitted electron beam to pass, as shown in Fig. 3.11. The bright-field image is observed at the detector or viewing screen. If the aperture is positioned to select only one of the beams reflected from a particular *hkl* plane, the result is the generation of a dark-field image at the viewing screen. The details of the dark-field image that is formed can depend on the particular diffracted beam (particular *hkl* plane) that is selected for the imaging. Figure 3.11 shows the locations of the bright-field (BF) and dark-field (DF) aperture positions. To illustrate this imaging technique we present in Fig. 3.12 images of an iron base superalloy with a FCC austenite structure containing 2–3-nm γ' preci-

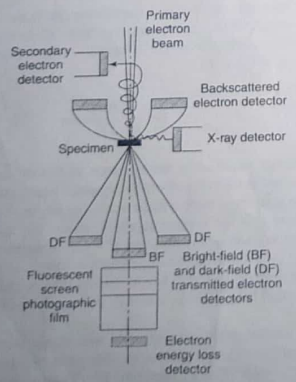

Figure 3.11. Positioning of signal detectors in electron microscope column. (From D. B. Williams, *Practical Analytical Electron Microscopy in Materials Science*, Phillips Electronic Instruments, Mahwah NJ, 1984.)

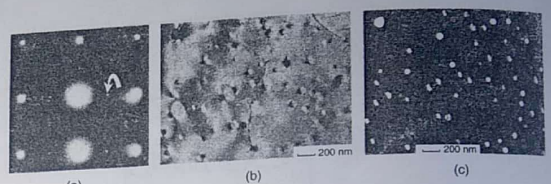

Figure 3.12. Transmission electron microscope figures from 2–3-nm-diameter γ' precipitates of Ni_3(Ti, Al) in iron-base superalloy, showing (a) [100] FCC zone diffraction pattern displaying large bright spots from the superalloy and weak spots from the γ' precipitates, (b) bright-field image showing 25-nm elastic strain fields around marginally visible γ' phase particles, and (c) dark-field image obtained using an SAED aperture to pass the γ' diffraction spot marked with the arrow in (a). Image (c) displays the γ' precipitate particles. [From T. J. Headley, cited in A. D. Romig, Jr., chapter in R. E. Whan (1986), p. 442.]

pitates of Ni_3(Ti, Al) with a FCC structure. The diffraction pattern in Fig. 3.12a obtained without the aid of the filter exhibits large, bright spots from the superalloy, and very small, dim spots from the γ' nanoparticles. In the bright-field image displayed in Fig. 3.12b the γ' particles are barely visible, but the 25-nm-diameter elastic strain fields generated by them are clearly seen. If the γ' diffraction spot beam indicated by the arrow in Fig. 3.12a is selected for passage by the SAED aperture, the resulting dark-field image presented in Fig. 3.12c shows very clearly the positions of the γ' precipitates.

A technique called image processing can be used to increase the information obtainable from a TEM image, and enhance some features that are close to the noise level. If the image is Fourier-transformed by a highly efficient technique called a *fast Fourier transform*, then it provides information similar to that in the direct diffraction pattern. An example of the advantages of image processing is given by the sequence of images presented in Fig. 3.13 for a Ni nanoparticle supported on a SiO_2 substrate. Figure 3.13a shows the original image, and Fig. 3.13b presents the fast Fourier transform, which has the appearance of a diffraction pattern. Figures 3.13c–3.13e illustrate successive steps in the image processing, and Fig. 3.13f is an image of the SiO_2 substrate obtained by subtracting the particle image. Finally Fig. 3.13g presents the nanoparticle reconstruction from the processed data.

In addition to the directly transmitted and the diffracted electrons, there are other electrons in the beam that undergo inelastic scattering and lose energy by creating excitations in the specimen. This can occur by inducing vibrational motions in the atoms near their path, and thereby creating phonons or quantized lattice vibrations that will propagate through the crystal. If the sample is a metal, then the incoming electron can scatter inelastically by producing a plasmon, which is a collective excitation of the free-electron gas in the conduction band. A third very important source of inelastic scattering occurs when the incoming electron induces a single-

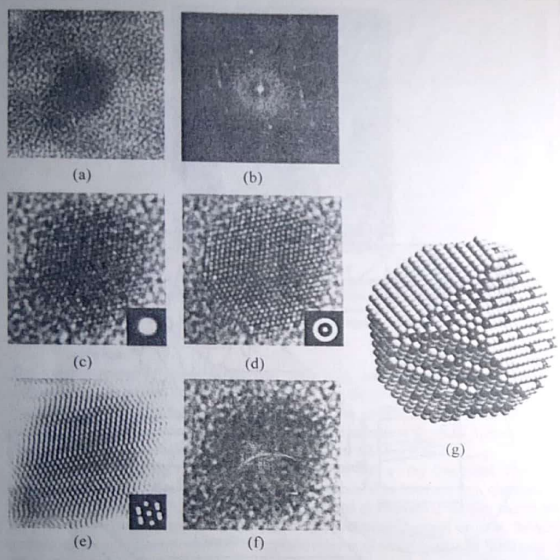

Figure 3.13. Transmission electron microscope image processing for a Ni particle on a SiO_2 substrate, showing (a) original bright-field image, (b) fast Fourier transform diffraction-pattern-type image, (c) processed image with aperture filter shown in inset, (d) image after further processing with aperture filter in the inset, (e) final processed image, (f) image of SiO_2 substrate obtained by subtracting out the particle image, and (g) model of nanoparticle constructed from the processed data. [From Benaissa and Diaz, cited by M. José-Yacamán and J. A. Ascencio, in Nalwa (2000), Vol. 2, Chapter 8, p. 405.]

electron excitation in an atom. This might involve inner core atomic levels of atoms, such as inducing a transition from a K level ($n = 1$) or L level ($n = 2$) of the atom to a higher energy that might be a discrete atomic level with a larger quantum number n, an electron band, or result in total removal (ionization) from the solid. Lower levels of energy loss occur when the excited electron is in the valence band of a semiconductor. This excitation can decay via the return of excited electrons to their ground states, thereby producing secondary radiation, and the nature of the secondary radiation can often give useful information about the sample. These

types of transitions are utilized in various branches of electron spectroscopy. They can be surface-sensitive because of the short penetration distance of the electrons into the material.

3.3.2. Field Ion Microscopy

Another instrumental technique in which the resolution approaches interatomic dimensions is field ion microscopy. In a field ion microscope a wire with a fine tip located in a high-vacuum chamber is given a positive charge. The electric field and electric field gradient in the neighborhood of the tip are both quite high, and residual gas molecules that come close to the tip become ionized by them, transferring electrons to the tip, thereby acquiring a positive charge. These gaseous cations are repelled by the tip and move directly outward toward a photographic plate where, on impact, they create spots. Each spot on the plate corresponds to an atom on the tip, so the distribution of dots on the photographic plate represents a highly enlarged image of the distribution of atoms on the tip. Figure 3.14 presents a field ion micrograph from a tungsten tip, and Fig. 3.15 provides a stereographic projection of a cubic crystal with the orientation corresponding to the micrograph of Fig. 3.14. The *International Tables for Crystallography*, edited by T. Hahn (Hahn 1996), provide stereographic projections for various point groups and crystal classes.

3.3.3. Scanning Microscopy

An efficient way to obtain images of the surface of a specimen is to scan the surface with an electron beam in a raster pattern, similar to the way an electron gun scans the

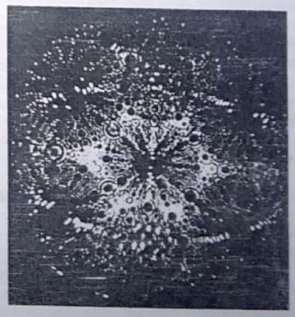

Figure 3.14. Field ion micrograph of a tungsten tip (T. J. Godfrey), explained by the stereographic projection of Fig. 3.15. [From G. D. W. Smith, chapter in Whan (1986), p. 585.]

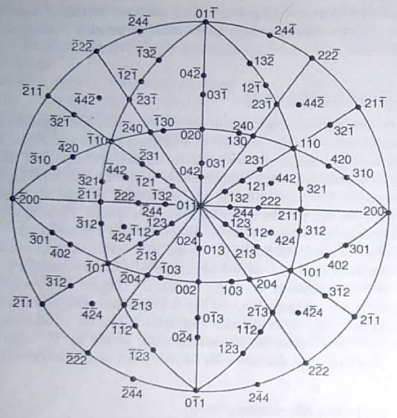

Figure 3.15. Stereographic [011] projection of a cubic crystal corresponding to the field ion tungsten micrograph in Fig. 3.14. [From G. D. W. Smith, chapter in Whan (1986), p. 583.]

screen in a television set. This is a systematic type scan. Surface information can also be obtained by a scanning probe in which the trajectory of the electron beam is directed across the regions of particular interest on the surface. The scanning can also be carried out by a probe that monitors electrons that tunnel between the surface and the probe tip, or by a probe that monitors the force exerted between the surface and the tip. We shall describe in turn the instrumentation systems that carry out these three respective functions: the scanning transmission electron microscope (SEM), the scanning tunneling microscope (STM), and the atomic force microscope (AFM).

It was mentioned above that the electron optics sketched in Fig. 3.10 for a conventional transmission electron microscope is similar to that of a scanning electron microscope, except that in the former TEM case the electrons travel from left to right, and in the latter SEM they move in the opposite direction, from right to left, in the figure. Since quite a bit has been said about the workings of an electron microscope, we describe only the electron deflection system of a scanning electron microscope, which is sketched in Fig. 3.16. The deflection is done magnetically through magnetic fields generated by electric currents flowing through coils, as

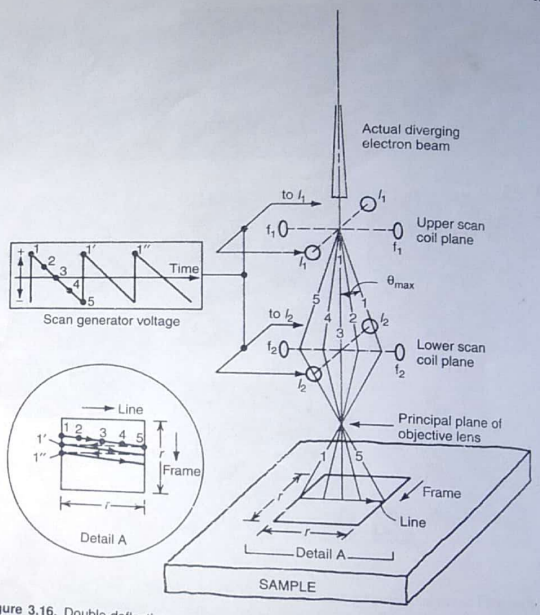

Figure 3.16. Double-deflection system of a scanning electron microscope. When the upper scan coils I_1–I_1 deflect the beam through an angle θ, the lower scan coils I_2–I_2 deflect it back through the angle 2θ, and the electrons sequentially strike the sample along the indicated line. The upper inset on the left shows the sawtooth voltage that controls the current through the I_1 scanning coils. The lower inset on the left shows the sequence of points on the sample for various electron trajectories 1, 2, 3, 4, 5 downward along the microscope axis. Scan coils f_1–f_1 and f_2–f_2 provide the beam deflection for the sequence of points 1, 1′, 1″ shown in detail A. [From J. D. Verhoeven, chapter in Whan (1986), p. 493.]

occurs in many television sets. The magnetic field produced by a coil is proportional to the voltage V applied to the coil. We see from the upper inset on the left side of Fig. 3.16 that a sawtooth voltage is applied to the pairs of coils I_1,I_1 and I_2,I_2. The magnetic field produced by the coils exerts a force that deflects the electron beam from left to right along the direction of the line drawn at the bottom on the sample.

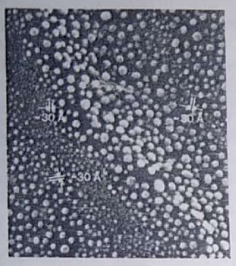

Figure 3.17. Micrograph of 3-nm-diameter (30-Å) gold particles on a carbon substrate taken with a scanning electron microscope. [From J. D. Verhoeven, chapter in Whan (1986), p. 497.]

The varying magnetic fields in the coil pairs f_1, f_1 and f_2, f_2 produce the smaller deflections from points 1 to 1′ to 1″ shown in the detail A inset. Thus the electron beam scans repeatedly from left to right across the sample in a raster pattern that eventually covers the entire $r \times r$ frame area on the sample. Figure 3.17 shows 3-nm gold particles on a carbon substrate resolved by an SEM.

A scanning tunneling microscope utilizes a wire with a very fine point. This fine point is positively charged and acts as a probe when it is lowered to a distance of about 1 nm above the surface under study. Electrons at individual surface atoms are attracted to the positive charge of the probe wire and jump (tunnel) up to it, thereby generating a weak electric current. The probe wire is scanned back and forth across the surface in a raster pattern, in either a constant-height mode, or a constant-current mode, in the arrangements sketched in Fig. 3.18. In the constant current mode a feedback loop maintains a constant probe height above the sample surface profile, and the up/down probe variations are recorded. This mode of operation assumes a constant tunneling barrier across the surface. In the constant-probe-height mode the tip is constantly changing its distance from the surface, and this is reflected in variations of the recorded tunneling current as the probe scans. The feedback loop establishes the initial probe height, and is then turned off during the scan. The scanning probe provides a mapping of the distribution of the atoms on the surface.

The STM often employs a piezoelectric tripod scanner, and an early design of this scanner, built by Binning and Rohrer, is depicted in Fig. 3.19. A piezoelectric is a material in which an applied voltage elicits a mechanical response, and the reverse. Applied voltages induce piezo transducers to move the scanning probe (or the sample) in nanometer increments along the x, y or z directions indicated on the arms (3) of the scanner in the figure. The initial setting is accomplished with the aid of a stepper motor and micrometer screws. The tunneling current, which varies expo-

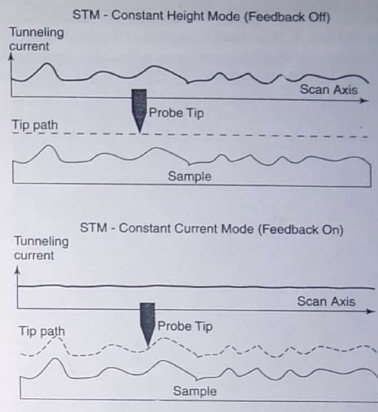

Figure 3.18. Constant-height (top sketch) and constant-current (bottom sketch) imaging mode of a scanning tunneling microscope. [From T. Bayburt, J. Carlson, B. Godfrey, M. Shank-Retzlaff, and S. G. Sligar, in Nalwa (2000), Vol. 5, Chapter 12, p. 641.]

nentially with the probe–surface atom separation, depends on the nature of the probe tip and the composition of the sample surface. From a quantum-mechanical point of view, the current depends on the dangling bond state of the tip apex atom and on the orbital states of the surface atoms.

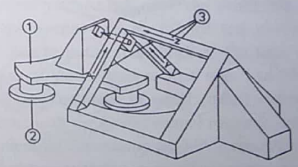

Figure 3.19. Scanning mechanism for scanning tunneling microscope, showing (1) the piezoelectric baseplate, (2) the three feet of the baseplate and (3) the piezoelectric tripod scanner holding the probe tip that points toward the sample. (From R. Wiesendanger, *Scanning Probe Microscopy and Spectroscopy*, Cambridge Univ. Press, Cambridge, UK, 1994, p. 81.)

The third technique in wide use for nanostructure surface studies is atomic force microscopy, and Fig. 3.20 presents a diagram of a typical atomic force microscope (AFM). The fundamental difference between the STM and the AFM is that the former monitors the electric tunneling current between the surface and the probe tip

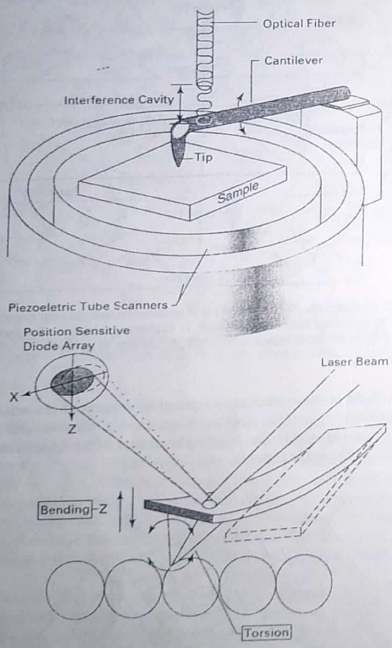

Figure 3.20. Sketch of an atomic force microscope (AFM) showing the cantilever arm provided with a probe tip that traverses the sample surface through the action of the piezoelectric scanner. The upper figure shows an interference deflection sensor, and the lower enlarged view of the cantilever and tip is provided with a laser beam deflection sensor. The sensors monitor the probe tip elevations upward from the surface during the scan.

and the latter monitors the force exerted between the surface and the probe tip. The AFM, like the STM, has two modes of operation. The AFM can operate in a close contact mode in which the core-to-core repulsive forces with the surface dominate, or in a greater separation "noncontact" mode in which the relevant force is the gradient of the van der Waals potential. As in the STM case, a piezoelectric scanner is used. The vertical motions of the tip during the scanning may be monitored by the interference pattern of a light beam from an optical fiber, as shown in the upper diagram of the figure, or by the reflection of a laser beam, as shown in the enlarged view of the probe tip in the lower diagram of the figure. The atomic force microscope is sensitive to the vertical component of the surface forces. A related but more versatile device called a *friction force microscope*, also sometimes referred to as a *lateral force microscope*, simultaneously measures both normal and lateral forces of the surface on the tip.

All three of these scanning microscopes can provide information on the topography and defect structure of a surface over distances close to the atomic scale. Figure 3.21 shows a three-dimensional rendering of an AFM image of chromium deposited on a surface of SiO_2. The surface was prepared by the laser-focused deposition of atomic chromium in the presence of a Gaussian standing wave that reproduced the observed regular array of peaks and valleys on the surface. When the laser-focused chromium deposition was carried out in the presence of two plane waves displaced by 90° relative to each other, the two-dimensional arrangement AFM image shown in Fig. 3.22 was obtained. Note that the separation between the peaks, 212.78 nm, is the same in both images. The peak heights are higher (13 nm) in the two-dimensional array (8 nm) than in the linear one.

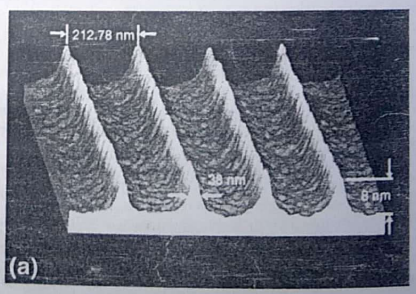

Figure 3.21. Three-dimensional rendering of an AFM image of nanostructure formed by laser focused atomic Cr deposition in a Gaussian standing wave on an SiO_2 surface. [From J. J. McClelland, R. Gupta, Z. J. Jabbour, and R. L. Celotta, *Aust J. Phys.* **49**, 555 (1996).]

Liposome is a spherical synthetic lipid bilayer vesicle, created in the laboratory by dispersion of a phospholipid in aqueous salt solutions. Liposome is quite similar to a micelle with an internal aqueous compartment. Liposomes, which are in nanoscale size range, as shown in Figure 9, self-assemble based on hydrophilic and hydrophobic properties and they encapsulate materials inside. Liposome vesicles can be used as carriers for a great variety of particles, such as small drug molecules, proteins, nucleotides and even plasmids to tissues and into cells. For example, a recent commercially available anticancer drug is a liposome, loaded with doxorubicin, and is approximately 100-nanometer in diameter.

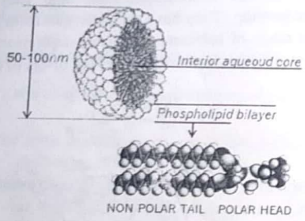

Figure 9. Cross section of a liposome - a synthetic lipid bilayer vesicle that fuses with the outer cell membrane and is used to transport small molecules to tissues and into cells.

A monoclonal antibody protein molecule consists of four protein chains, two heavys and two lights, which are folded to form a Y-shaped structure (see Figure 10). It is about ten nanometers in diameter. This small size is important, for example, to ensure that intravenously administered these particles can penetrate small capillaries and reach cells in tissues where they are needed for treatment. Nanostructures smaller than 20 *nm* can transit out of blood vessels.

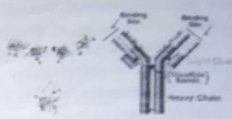

Figure 10. An antibody is a protein (also called an immunoglobulin) that is manufactured by lymphocytes (a type of white blood cell) to neutralize an antigen or foreign protein.

Ongoing Research and Development Activities

The atomic-scale and cutting-edge field of nanotechnology which is considered to lead us to the next industrial revolution is likely to have a revolutionary impact on the way things will be done, designed and manufactured in the future.

Nanotechnology is entering into all aspects of science and technology including, but not limited to, aerospace, agriculture, bioengineering, biology, energy, the environment, materials, manufacturing, medicine, military science and technology. It is truly an atomic and molecular manufacturing approach for building chemically and physically stable structures one atom or one molecule at a time. Presently some of the active nanotechnology research areas include nanolithography, nanodevices, nanorobotics, nanocomputers, nanopowders, nanostructured catalysts and nanoporous materials, molecular manufacturing, diamondoids, carbon nanotube and fullerene products, nanolayers, molecular nanotechnology, nanomedicine, nanobiology, organic nanostructures to name a few.

We have known for many years that several existing technologies depend crucially on processes that take place on the nanoscale. Adsorption, lithography, ion-exchange, catalysis, drug design, plastics and composites are some examples of such technologies. The "nano" aspect of these technologies was not known and, for the most part, they were initiated accidentally by mere luck. They were further developed

using tedious trial-and-error laboratory techniques due to the limited ability of the times to probe and control matter on nanoscale. Investigations at nanoscale were left behind as compared to micro and macro length scales because significant developments of the nanoscale investigative tools have been made only recently.

The above mentioned technologies, and more, stand to be improved vastly as the methods of nanotechnology develop. Such methods include the possibility to control the arrangement of atoms inside a particular molecule and, as a result, the ability to organize and control matter simultaneously on several length scales. The developing concepts of nanotechnology seem pervasive and broad. It is expected to influence every area of science and technology, in ways that are clearly unpredictable.

Nanotechnology will also help solve other technology and science problems. For example, we are just now starting to realize the benefits that nanostructuring can bring to,

(a) wear-resistant tires made by combining nanoscale particles of inorganic clays with polymers as well as other nanoparticle reinforced materials,
(b) greatly improved printing brought about by nanoscale particles that have the best properties of both dyes and pigments as well as advanced ink jet systems,
(c) vastly improved new generation of lasers, magnetic disk heads, nanolayers with selective optical barriers and systems on a chip made by controlling layer thickness to better than a nanometer,
(d) design of advanced chemical and bio-detectors,
(e) nanoparticles to be used in medicine with vastly advanced drug delivery and drug targeting capabilities,
(f) chemical-mechanical polishing with nanoparticle slurries, hard coatings and high hardness cutting tools.

The following selected observations regarding the expected future advances are also worth mentioning at this juncture [6]:

(A) The most complex arrangements of matter known to us are those of living entities and organs. Functions of living organisms depend on specific patterns of matter on all various length scales. Methods of nanotechnology could provide a new dimension to the control and improvement of living organisms.

(B) Photolithographic patterning of matter on the micro scale has led to the revolution in microelectronics over the past few decades. With nanotechnology, it will become possible to control matter on every important length scale, enabling tremendous new power in materials design.
(C) Biotechnology is expected to be influenced by nanotechnology greatly in a couple of decades. It is anticipated that, for example, this will revolutionize healthcare to produce ingestible systems that will be harmlessly flushed from the body if the patient is healthy but will notify a physician of the type and location of diseased cells and organs if there are problems.
(D) Micro and macro systems constructed of nanoscale components are expected to have entirely new properties that have never before been identified in nature. As a result, by altering and design of the structure of materials in the nanoscale range we would be able to systematically and appreciably modify or change selected properties of matter at macro and micro scales. This would include, for example, production of polymers or composites with most desirable properties which nature and existing technologies are incapable of producing.
(E) Robotic spacecraft that weigh only a few pounds will be sent out to explore the solar system, and perhaps even the nearest stars. Nanoscale traps will be constructed that will be able to remove pollutants from the environment and deactivate chemical warfare agents. Computers with the capabilities of current workstations will be the size of a grain of sand and will be able to operate for decades with the equivalent of a single wristwatch battery.
(F) There are many more observations in the areas of inks and dyes, protective coatings, dispersions with optoelectronic properties, nanostructured catalysts, high reactivity reagents, medicine, electronics, structural materials, diamondoids, carbon nanotube and fullerene products and energy conversion, conservation, storage and usage which are also worth mentioning.
(G) Many large organic molecules are known to forming organic nanostructures of various shapes as shown in Figures 5 and 11 the